npj | quantum materials

Article

Published in partnership with Nanjing University

https://doi.org/10.1038/s41535-025-00787-y

Universal approach to light driven "superconductivity" via preformed pairs

Ke Wang[1] ✉, Zhiqiang Wang[1,2,3,4], Qijin Chen[2,3,4] & K. Levin[1]

While there are many different mechanisms which have been proposed to understand the physics behind light induced "superconductivity", what seems to be common to the class of materials in which this is observed are strong pairing correlations, which are present in the normal state. Here we argue, that the original ideas of Eliashberg are applicable to such a pseudogap phase and that with exposure to radiation the fermions are redistributed to higher energies where they are less deleterious to pairing. What results then is a photo-induced state with dramatically enhanced number of nearly condensed fermion pairs. In this phase, because the a.c. conductivity, $\sigma(\omega) = \sigma_1(\omega) + i\sigma_2(\omega)$, is dominated by the bosonic contribution, it can be computed using conventional (Aslamazov Larkin) fluctuation theory. We, thereby, observe the expected fingerprint of this photoinduced "superconducting" state which is a $1/\omega$ dependence in σ_2 with fits to the data of the same quality as found for the so-called photo-enhanced (Drude) conductivity scenario. Here, however, we have a microscopic understanding of the characteristic low energy scale which appears in transport and which is necessarily temperature dependent. This approach also provides insight into recent observations of concomitant diamagnetic fluctuations. Our calculations suggest that the observed light-induced phase in these strongly paired superconductors has only short range phase coherence without long range superconducting order.

The phenomenon of light induced phase and structural transitions[1,2] and more specifically light induced, transient superconductivity well above T_c, has generated enormous excitement in the community[3–7]. In these latter experiments, a very fast, laser pulse of sub-picosecond (ps) duration is applied, and with a delay of around 1 to 10 ps the system is probed and the conductivity at mid-infrared and terahertz frequencies is measured. What is observed are superconducting-like signatures appearing in the normal state. Most notable among these is a low frequency upturn in the imaginary conductivity $\sigma_2(\omega)$, not so different from the $1/\omega$ dependence of a true superconductor.

In this paper we argue, as has Uemura[8], that, while there are many different mechanisms[9–26] suggested to explain these transient superconducting-like properties of matter, there seem to be important experimental commonalities. In particular, these transient light induced indications of superconductivity are observed at often high temperatures associated with a normal state that contains preformed pairs[5,17,27].

The goal of this paper is to build on these commonalities and to propose a more universal mechanism for such light induced phenomena, with an emphasis on addressing transport signatures in more quantitative detail. Here we note that in a strong pairing scenario such as we consider[28,29], we should view these preformed pairs as necessarily co-existing with (pseudo)gapped fermions. The fermions which are present along with preformed pairs play a central role in understanding these experiments, as they provide an important handle for implementing the physics of a highly non-equilibrium Eliashberg-like scenario[30] for light-enhanced superconductivity.

The Eliashberg picture begins with the premise that radiation promotes the gapped fermionic quasiparticles to higher energies, which is associated with a larger pairing gap. We have no well established tools for treating such highly non-equilibrium behavior, but it is claimed that there is no doubt that the Eliashberg effect exists[31]. What we address here is its application and generalization to the normal (non-superconducting) phase. In the Eliashberg scenario below T_c one views the quasiparticles as out of equilibrium with condensed Cooper pairs. Similarly, for the above T_c counterpart one views the quasiparticles as out of equilibrium with preformed pairs. It was previously found that in the Eliashberg scenario there is a substantial enhancement[32,33] of the transition temperature T_c. For the normal state in our theory we find a substantial enhancement of the counterpart pairing

[1]Department of Physics ad James Franck Institute, University of Chicago, Chicago, Illinois, USA. [2]Hefei National Research Center for Physical Sciences at the Microscale and School of Physical Sciences, University of Science and Technology of China, Hefei, Anhui, China. [3]Shanghai Research Center for Quantum Science and CAS Center for Excellence in Quantum Information and Quantum Physics, University of Science and Technology of China, Shanghai, China. [4]Hefei National Laboratory, University of Science and Technology of China, Hefei, China. ✉e-mail: kewang07@uchicago.edu

onset temperature T^*. A consequence is that, as the number of relevant fermionic excitations effectively decreases, this leads to an increase in both the gap size and the boson number, which will, in turn, have important implications for the normal state transport properties.

An important component of these experiments[5] are resonant phonons which initiate these "superconducting"-like responses to light. Exciting these particular phonons is important presumably because they serve to select the specific *fermions* which participate in the pairing. We argue that what is responsible for facilitating this non-equilibrium fermion redistribution is not the direct interaction between the photons and fermions, which has less specificity, but rather the direct interaction between the fermions and selected phonons. Indeed, an extended version of Eliashberg theory in which the enhancement mechanism is based on phonon absorption is now well established[34,35]. Adding support is the observation that, for example in the cuprates, the transition temperature seems to depend rather sensitively on the oxygen apical mode [36]. Similarly, exciting this mode has been found to be effective in initiating the light-enhanced behavior.

The physical picture associated with the Eliashberg mechanism in the normal state is schematically represented in Fig. 1. As has been pointed out[32] one can interpret this mechanism more microscopically as being associated with a radiation-induced increase in the strength of the attractive interaction. It is important to emphasize that this increase in the attraction only occurs by redistribution of fermions. It is not related to the microscopic details of the pairing mechanism which leads to the superconductivity. Because it occurs in the normal state, this leads to enhanced signatures of precursor (fluctuation) superconductivity.

Our recent review[28] provided an overview of these strongly paired superconductors. Interestingly among materials which exhibit light enhanced "superconductivity" are

1. Members of the cuprate family [4,5].
2. Members of the Fe-Se family[37].
3. A particular organic superconductor[38], known as κ-BEDT-TTF.
4. A particular fulleride [5,39] K_3C_{60}.All of these we identified as strongly paired except for the fulleride, but it now appears that this one notable example (K_3C_{60}) also seems to belong to this category[40]. We found additional strong pairing superconductors belonging to the class of artificial materials[41,42] which have not been addressed in pump-probe experiments. Otherwise the overlap between those we identified and those which exhibit this transient superconductivity is surprisingly good.

Preformed pairs in generalized BCS theory

The strongly-paired superconductor scenario[28,29] depends on an enhanced pairing strength, beyond that associated with the BCS regime. There are two characteristic temperatures in such a superconductor: T^* and T_c. Here T^*, introduced earlier, represents the onset temperature for the opening of a gap, while T_c represents the ordering or phase coherence temperature. The excitations are pseudogapped fermions (having a Bogoliubov-like dispersion) as well as non-condensed or preformed pairs at $T < T^*$. The gap parameter Δ takes on a different character above and below T_c. Above T_c, which is of primary interest here, $\Delta \equiv \Delta_{pg}$, where "pg" refers to the pseudogap.

To understand the nature of preformed pairs within a generalized BCS formalism, it is useful to recognize that the BCS gap equation can be written compactly in terms of the Gor'kov function $F(k) \equiv \Delta G(k)G_0(-k) = \Delta/(\omega_n^2 + E_{\mathbf{k}}^2)$, where $G(k) = (i\omega_n + \xi_{\mathbf{k}})/(-\omega_n^2 - E_{\mathbf{k}}^2)$ is the usual (diagonal) Gor'kov Green's function, and $E_{\mathbf{k}} = \sqrt{\xi_{\mathbf{k}}^2 + \Delta^2(T)}$ is the gapped fermionic quasiparticle dispersion. $G_0(k) = (i\omega_n - \xi_{\mathbf{k}})^{-1}$ and $k = (i\omega_n, \mathbf{k})$, with $\omega_n = (2n+1)\pi T$ the fermionic Matsubara frequency. We have adopted the units $\hbar = k_B = c = 1$. Note that for simplicity, we drop here the order parameter symmetry multiplier, $\varphi_{\mathbf{k}}$, (which would take the form $\varphi_{\mathbf{k}} = \cos k_x - \cos k_y$ for a systems with d-wave pairing). Using these Green's functions we can write the gap equation as

$$\begin{aligned} \Delta(T) &= U \sum_k F(k) \\ \Rightarrow 0 &= \left[-U^{-1} + \sum_k G(k)G_0(-k) \right] \Delta(T), \end{aligned} \tag{1}$$

where $U > 0$ is the attraction strength and $\sum_k \equiv T\sum_n \sum_{\mathbf{k}}$. This form motivates a natural choice for the pair propagator or t-matrix, characterizing the non-condensed or preformed pairs, which has been discussed in the literature[43]

$$t^{-1}(q) = \sum_k G(k)G_0(q-k) - U^{-1}, \tag{2}$$

where $q = (i\Omega_m, \mathbf{q})$ with $\Omega_m = 2m\pi T$ the bosonic Matsubara frequency, and $m \in \mathcal{Z}$. We can view the gap equation below T_c as equivalent to the requirement that $t^{-1}(0) = 0$ while above T_c, $t^{-1}(0) = Z\mu_{\text{pair}} \neq 0$ where Z is a coefficient of proportionality that arises when expanding $t^{-1}(\Omega, \mathbf{q} = 0) - t^{-1}(0)$ at small $|\Omega|$. This introduces a key parameter, μ_{pair}, which represents the chemical potential of the pairs and which identically vanishes at and below T_c, as expected of a (Bose Einstein) condensation. It should be emphasized that this asymmetric combination of G_0G is derived rigorously from the equations of motion for the Green's function series and is not an ad hoc choice.

Thus, in the normal state, we have that

$$t^{-1}(0) = \sum_{\mathbf{k}} \frac{1 - 2f(E_{\mathbf{k}})}{2E_{\mathbf{k}}} - U^{-1} = Z\mu_{\text{pair}}, \tag{3}$$

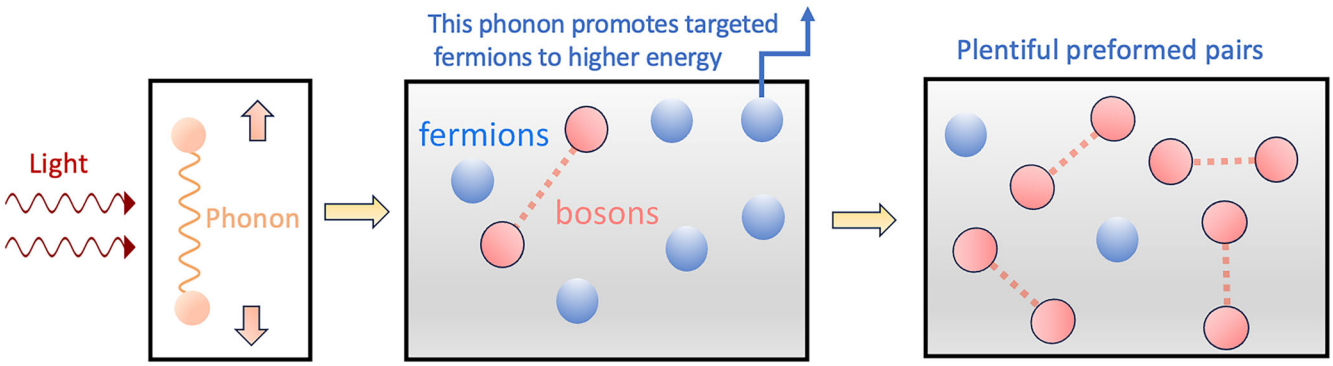

Fig. 1 | This figure represents a simple physical picture of the Eliashberg mechanism now extended to the normal phase. The effects of light (indirectly through a specially selected phonon) serve to redistribute those particular fermions associated with superconductivity to higher energies[34,35], As a consequence, after radiation, while the fermion number is substantially reduced, the pairing is strengthened and preformed pairs (bosons) become more plentiful, thus leading to enhanced fluctuation transport signatures.

where $f(x) = 1/(e^{\beta x} + 1)$ is the Fermi-Dirac distribution function. Equation (3) can be used to determine $\mu_{\rm pair}$ provided one knows $\Delta_{\rm pg}$, which can be obtained in terms of the number of preformed pairs, n_B, in the system. Here n_B is to a good approximation given by

$$n_B = \sum_{\mathbf{q}} b\left(\frac{\mathbf{q}^2}{2M_B} - \mu_{\rm pair}\right) = Z\Delta_{\rm pg}^2, \tag{4}$$

where $b(x) = 1/(e^{\beta x} - 1)$ is the Bose-Einstein distribution. The pair dispersion $\mathbf{q}^2/2M_B$ or equivalently the pair mass M_B and all parameters in the t-matrix, such as Z, can be obtained[28] by a small q expansion of Eq. (2). In determining these parameters one must similarly solve self-consistently for the fermionic chemical potential μ. The equations to be solved are those at equilibrium, which depend on the usual Fermi distribution function $f(E_{\mathbf{k}})$.

In the presence of EM radiation, we contemplate, within the Eliashberg scenario[30], that there is a redistribution of the gapped fermionic quasiparticles to higher energies. As a result, the key parameters $\mu_{\rm pair}$ and n_B and $\Delta_{\rm pg}$ as well all are altered. If the temperature is unchanged, such a momentum space redistribution of fermions is to be associated with an increased Δ (and accordingly lowered chemical potential μ) as the system tries to re-equilibrate. This, then, leads to a stronger pairing.

To understand how, we can make some useful inferences[32] here by writing

$$f(E_{\mathbf{k}}) \to \tilde{f}(E_{\mathbf{k}}) = f(E_{\mathbf{k}}) - \delta f(E_{\mathbf{k}}),$$

in the energy regime where pairing takes place. Here $\delta f(E_{\mathbf{k}})$ represents a change in the distribution of fermions. We assume that, after the radiation, the system is in a quasi-equilibrated state where the new distribution of fermionic excitations, $\tilde{f}(E_{\mathbf{k}})$, satisfies an equation similar to Eq. (3), which leads to

$$\sum_{\mathbf{k}} \frac{1 - 2\tilde{f}(E_{\mathbf{k}})}{2E_{\mathbf{k}}} - U^{-1} = Z\mu_{\rm pair}. \tag{5}$$

By rewriting this equation in the form of Eq. (3) with the equilibrium $f(E_{\mathbf{k}})$, we can see that the interaction term U, which is large to begin with, is effectively strengthened by the redistribution of the gapped fermionic excitations. These effects can be incorporated into a renormalized interaction, $U_{\rm eff}$, given by

$$\frac{1}{U_{\rm eff}} = \frac{1}{U} - \sum_{\mathbf{k}} \frac{2\delta f(E_k)}{2E_{\mathbf{k}}} \tag{6}$$

The summation in Eq. (6) must necessarily be positive as required by the shifted momentum space fermion redistribution. Importantly, this increase which appears in $U_{\rm eff}$ will raise the pairing onset temperature, T^*. There is no simple direct equation which focuses on this temperature, but it can be approximated using the mean field BCS gap equation, in the limit $\Delta \to 0$. As might be expected [32], in this case, the increase in $U_{\rm eff}$ will enter exponentially as an enhancement of the characteristic temperature. A more detailed implementation of these ideas can be found in Ref. 44, albeit in the context of a light-enhanced superconducting, rather than pseudogap phase as discussed here. There are bounds on how large these effects can be as the number of fermions that are redistributed can not exceed those that are initially present.

Interestingly, we can infer that the radiation exposure and subsequent redistribution of the fermions will likely lead to a *decrease* in T_c, as $U_{\rm eff}$ gets strongly enhanced. This latter, well-known [45] observation is associated with a superconducting dome-like phase diagram in which T_c is necessarily non-monotonic with varying T^*. The final state after radiation is to be associated with the stronger-coupling side of the T_c dome in this phase diagram[28]. In a related fashion the redistribution of fermions, now applied to the pseudogap phase, leads as well to a *decrease* in the magnitude of $|\mu_{\rm pair}|$ and an increase in the number of bosons, n_B.

Importantly, for the purposes of the present paper, these observations imply that there will be an enhancement in the (bosonic) fluctuation transport contributions. These are to be associated with Aslamazov-Larkin contributions and are seen to contribute when the temperature is considerably below the gap onset temperature[46], T^*. The signature of light-enhanced "superconductivity" is based on the behavior of the imaginary contribution to $\sigma(\omega) = \sigma_1 + i\sigma_2$, where a $1/\omega$ dependence is crucial. We address the counterpart calculations of $\sigma(\omega)$ in the Methods section, where we implement the known pairing fluctuation contributions to this transport [46,47]. Under radiation exposure, we expect that the number of fermion pairs is dramatically enhanced and the bosonic contribution will dominate the ac conductivity. This provides a normalization for $\sigma_1(\omega)$ in terms of the measured plasma frequency, ω_p.

Results

To address this transport behavior, in Fig. 2a we present a prototypical equilibrium phase diagram for the behavior of T^* and T_c, here for the case of the cuprate superconductors. We should point out there are changes in the carrier density across this phase diagram, which are not relevant. Nevertheless, one can see from Fig. 8 in Ref. 28 that the cuprate phase diagram is rather typical. A similar T_c dome structure is seen in the organic superconductor[48], which compound is also associated with light-induced "superconductivity", but there T^* was not addressed. In the right panel of Fig. 2, we have indicated the behavior of the pair chemical potential for a selected set of strongly paired superconductors with the same color codes as shown in the phase diagram.

The effects of radiation lead to a substantial increase of T^*. And we here presume this happens at a constant temperature. We illustrate how transport is affected by taking as the final state one with high T^* shown by the blue triangle in the phase diagram of Fig. 2a corresponding to the blue curve in Fig. 2b. A range of initial states before radiation can be contemplated, say corresponding to those indicated by the colored triangles on the T_c dome, with their respective smaller T^*. The most pronounced change in the conductivity will occur if the initial state corresponds to the red triangle, which is the case we consider here for illustrative purposes. This initial state, before radiation, of course, is of lesser importance.

In Fig. 3 we compare the behavior of σ_2 before and after radiation. This is to be associated with the transition shown in Fig. 2 by the brown arrow, from the red to blue curves, as T^*/T_c changes from 1.2 to 15 reflecting an increase in the strength of the pairing interaction. Also indicated in Fig. 3 is the behavior associated with a counterpart superconductor (blue dashed curve) and the characteristic range of frequencies accessible experimentally. One sees that the σ_2 obtained after radiation for the preformed pairs behaves quite similarly to the superconducting σ_2 for those frequencies which are accessible to experiments.

It is important to stress that there are somewhat closely related but competing ideas in the literature arguing that what is being observed experimentally cannot readily distinguish the superconducting state from a non-superconductor. This is principally due to the limitation of accessible frequencies. In this alternative scenario, rather than the non-interacting bosons discussed here one considers non-interacting fermions whose conductivity is described by Drude theory[49,50]. There one assumes that under exposure to radiation the fermionic lifetime τ becomes extremely long, thereby providing an alternative low energy scale. If one takes comparable parameters for $|\mu_{\rm pair}|$ and τ^{-1}. the frequency dependent conductivity will be very similar to the present case.

A comparison between these boson and fermion theories, using physical units is presented in Fig. 4, for both the real and imaginary components of the conductivity. For definiteness, in the Drude fits, previous work[49,50] suggested that τ^{-1} might vary between 0.6 and 1.2 meV. Here we chose 1.2meV for the plots. It is important to note that the real part vanishes more rapidly than the imaginary term in the high frequency regime. Rather than following the power law $1/\omega$ as in σ_2, σ_1 falls off more rapidly with ω, as the

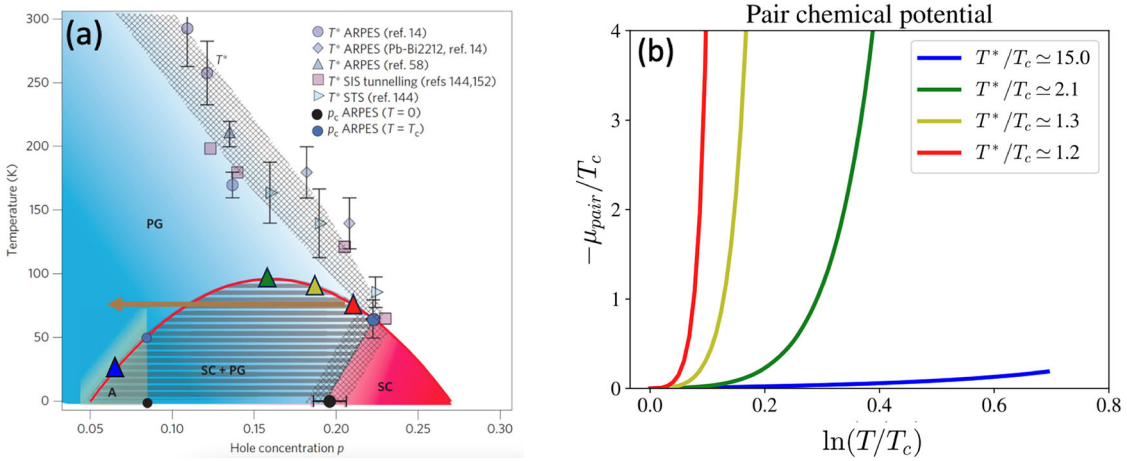

Fig. 2 | The figure presents a prototypical phase diagram of strongly coupled superconductors and the associated pair chemical potential of these states. **a** Shows a prototypical phase diagram for superconductors with strong pairing, in this case for the cuprate[59]. Indicated is the T_c dome, along with the pairing onset temperature T^*. The latter reflects the size of the attractive interaction. This figure represents the effect of changing the attractive interaction (at small T^*/T_c) so that (as in the brown arrow) a state shown by the red triangle can be transformed to a state associated with the blue triangle (at larger T^*/T_c) while keeping the temperature the same. The left-hand edge of the dome corresponds to a relatively strong interaction strength. **b** Shows the behavior of the bosonic chemical potential for the analogous superconductors associated with the same color codes as for the triangles in (**a**). Note that systems with larger attraction (larger T^*/T_c) have smaller $|\mu_{\text{pair}}|$ over a more extended range of temperatures.

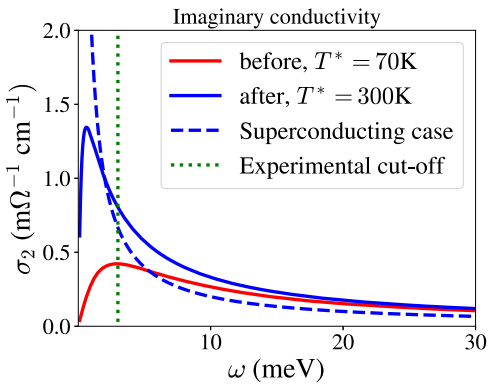

Fig. 3 | This shows the changes in $\sigma_2(\omega)$ before (red) and after (blue) exposure to radiation. The dotted green line indicates the lower frequency cut-off set by the experiments. This figure indicates how the signature upturn in $\sigma_2(\omega)$ is enhanced by the effective increase in T^* associated with exposure to radiation. The blue line can be compared with a typical superconductor, presuming, for example a superfluid density ratio of $n_s/n \approx 0.6$.

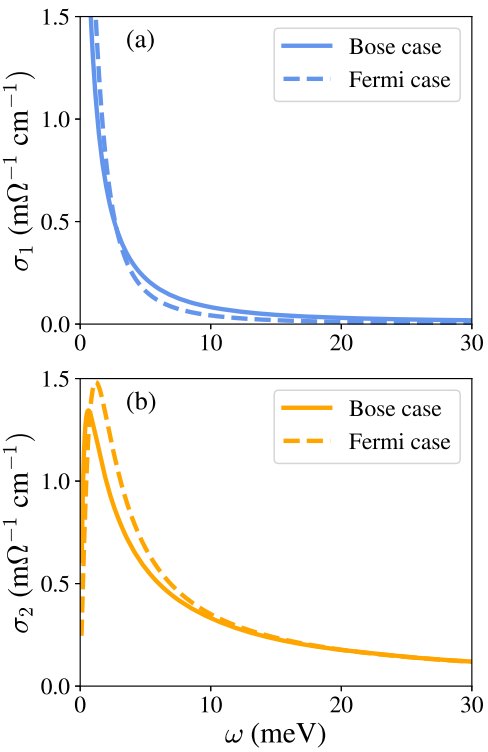

Fig. 4 | This shows a comparison between Fermi (Drude) and Bose conductivities. **a** Plots the real part of the conductivity, and **b** plots the imaginary counterpart. As long as the characteristic (low) energy scales are similar, the transport properties are also comparable. Note also that σ1 (ω) is quite a bit smaller in the relevant frequency range, than σ2 (ω). The computed values in the range varying from 3 meV to around 10 meV, are in reasonable agreement with the experiment.

f-sum rule is exhausted by the weight of σ_1 at small frequency due to the small energy scale, $|\mu_{\text{pair}}|$ or τ^{-1}. This is also compatible with light-induced experiments – that after radiation for a range of higher frequencies, there is very little contribution to $\sigma_1(\omega)$.

Importantly, the absolute values deduced for the real and imaginary conductivities in both theories are in reasonable agreement with the experimental values. This is the case provided the analysis is based on the protocol from ref. 49 which takes into account some of the complications about the pump-probe profile deformations which were not included in the original studies.

This raises the next question of how to distinguish between the photoenhanced conductivity and the present preformed pair scenario. To do so, we consider the effects of varying temperature as well as accompanying diamagnetism, both of which play a rather important role in the bosonic transport scenario, but do not appear as relevant for the Drude model. Plotted on the left in Fig. 5 is the temperature variation of $\omega\sigma_2(\omega)$ for one particular frequency and for the same system considered in Fig. 3; here the lowest temperature corresponds to $\sigma_2(\omega) \approx \frac{ne^2}{m\omega}$, while at higher T, $\omega\sigma_2$ becomes progressively reduced. This can be compared with Fig. 5 in Ref. 51. The counterpart diamagnetic susceptibility $\chi_{\text{dia}} \propto -\frac{T}{|\mu_{\text{pair}}|}$, here estimated for a quasi-two-dimensional (2d) system, is plotted in panel (b) for these same temperatures.

These figures show that temperature (through μ_{pair}) plays a rather profound role in bosonic fluctuation transport. This, presumably, is harder to argue for in the alternative fermionic scenario. Interestingly, temperature

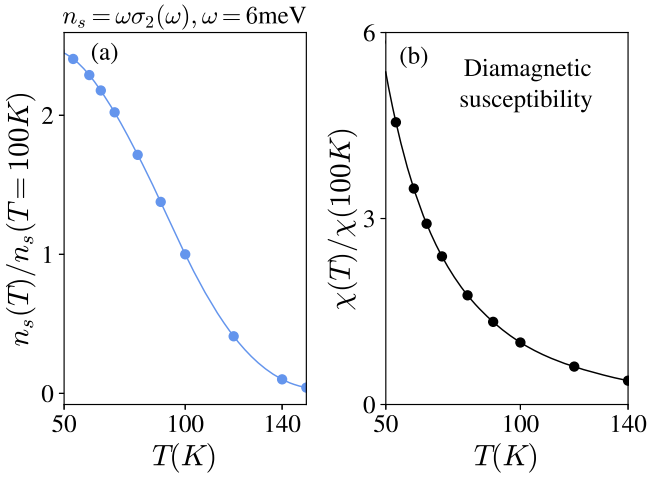

Fig. 5 | The figure shows the temperature dependence of the effective superfluid density and the diamagnetic susceptibility. a plots $\omega\sigma_2$ (ω) at 6meV for different initial temperatures and should be compared with Fig. 5 in ref. 51. **b** Plots the corresponding diamagnetic susceptibility for the same temperatures. Note that neither plot has contributions which extend all the way to the temperature $T^* \approx 300$K, although that seems to be the case in the experiments.

is also important in these light-driven experiments[51,52]. What is plotted in Fig. 5b is the temperature-dependent diamagnetic susceptibility, which is somewhat different from the experimental magnetic expulsion plot. Nevertheless, these figures make clear that the enhanced diamagnetism found here is directly correlated with the peak structure in the optical conductivity.

Discussion

A central goal of this paper was to present a more universal scenario for the phenomenon of light-enhanced "superconductivity". The materials where this is observed seem to nicely overlap with those which are associated with stronger than BCS pairing[28], such as the particular fulleride– K_3C_{60}, and organic superconductor–$\kappa-$ BEDT-TTF as well as members of the cuprate and Fe-Se families.

In this context, it should be noted that the "strong pairing glue", preformed pair scenario which we present here, can be put in the context of the widely discussed "phase fluctuation picture"[53]. In this latter approach, it is claimed that "phonon excitation may transfer phase coherence to the preformed pairs." Here we present a more microscopic linkage which emphasizes the role of fermions: specific phonons help to target those fermions that participate in the pairing. This, in turn, causes their redistribution to higher energies and thereby (as in the Eliashberg mechanism[30,34,35]) enhances pairing.

While we have emphasized the implications for transport from the bosonic perspective, this reduction in fermion number will also affect the measured transport directly. In particular, for the diamagnetic signal, well-known paramagnetic contributions from Pauli and from the larger[54] orbital Van Vleck mechanism[55] will be mostly removed, thereby leading to even more enhanced diamagnetism than was estimated here. In this sense, a light induced state should be viewed as a new phase of matter. It is associated with a removal of a large fraction of the fermions, making it different from, say, the preformed pair state in an equilibrated, underdoped (large T^*) cuprate.

Methods

The AC Conductivity of Preformed Pairs

We focus on pairing fluctuation contributions to the transport,[46,47], where the ac conductivity $\sigma(\omega)$ *in the normal state* is given by

$$\sigma_{ij}(\omega) = 4\frac{ie^2}{\omega}\int\frac{d\mathbf{q}}{(2\pi)^d}\frac{d\omega'}{2\pi}v_i(\mathbf{q})v_j(\mathbf{q})A(\mathbf{q},\omega')b(\omega') \times Z\left[t(\mathbf{q},\omega'+\omega)+t^*(\mathbf{q},\omega'-\omega)-t(\mathbf{q},\omega')-t^*(\mathbf{q},\omega')\right]. \quad (7)$$

Here $Zt(\mathbf{q}, \omega)$ is the (retarded) pair propagator, d represents the spatial dimension of the system which we take to be quasi-2d. $A(\mathbf{q}, \omega) = \text{Re}[2iZt(\mathbf{q}, \omega)]$ is the boson spectral function and $v_i(\mathbf{q}) = q_i/M_B$ is the boson velocity along the ith-direction; for the quasi-2d system we consider, we take $\sigma(\omega)$ to be the diagonal (and isotropic) in-plane component of σ_{ij}.

It is important to stress that dominating this transport is the generally small parameter $|\mu_{\text{pair}}|$, which sets the scale for divergences and other features[47]. Knowing that $\sigma(\omega)$ is governed by a very low temperature scale, it follows that the imaginary part of the conductivity at moderate frequencies, $\omega \gg |\mu_{\text{pair}}(T)|$, will behave quite universally as $\sigma_2(\omega) \approx \frac{ne^2}{m\omega}$. Here n/m is the effective fermionic number density to mass ratio.

In order to convert to realistic units, we assume that under radiation exposure, the bosonic contribution dominates the ac conductivity and thus will exhaust the f-sum rule. This provides a normalization for $\sigma_1(\omega)$ in terms of the measured plasma frequency, ω_p. Throughout, we will use the experimental value for this plasma frequency, ω_p = 160 meV, taken from Refs. 49 and 50. This is chosen to be representative of a prototypical material which manifests light-enhanced "superconductivity" (Here, in addition it is useful to convert conductivity to conventional units via $e^2/(\hbar d) = 1.58 \times 10^5\ \Omega^{-1}m^{-1}$ where we take[56] for a quasi-2d system, with an inter-layer spacing d = 1.54 nm.).

Since we are interested in a wide range of frequencies, the fully self-consistent integral expression in Eq. (2) is cumbersome to use for the t-matrix appearing in the conductivity equation Eq. (7). Thus, for the purposes of transport, we will consider a simple, generic boson propagator given by

$$Zt(\mathbf{q},\omega) \equiv \left[\omega - \Sigma_1(\omega) - \frac{\mathbf{q}^2}{2M_B} - \mu_{\text{pair}} + \frac{i}{2}\Sigma_2(\omega)\right]^{-1}. \quad (8)$$

The specific details of these self-energy parameters are not important and do not affect the conclusions (Here, as in Ref. 46, we take $\Sigma_1(\omega), \Sigma_2(\omega) \propto \omega$ with prefactors < 1 and a smaller prefactor for this second parameter).

As an additional approximation, it is useful for our purposes to obtain a more analytical expression for the centrally important pair chemical potential μ_{pair} in terms of T_c and T^*. We find our more detailed numerical calculations in an equilibrium system[57] are reasonably well fitted, as plotted in Fig. 2 (right panel), by $-\mu_{\text{pair}} = \frac{8}{\pi\eta}(T - T_c) + \alpha\frac{(T-T_c)^3}{(T^*-T)^2}$, with fitted parameters η and α. Here we take $\eta \approx 10 - 20$ and $\alpha \approx 15$. Necessarily, μ_{pair} vanishes at T_c and reaches $-\infty$ at T^* where the bosons disappear.

Figure6 is included to indicate the various energy scales which appear in a prototypical BCS-BEC phase diagram [28], here, for concreteness, shown for the cuprates. Plotted is the phase diagram which includes the data of Figure 2a indicating the temperature scales T^* and T_c. As can be seen unlike T_c, T^* is monotonic and uniquely associated with a distinct superconductor. Importantly, this temperature is not directly relevant to our transport considerations, as enhanced conductivity behavior is only to be expected when the pair chemical potential (shown in Fig. 2b) is small, which is the case much closer to T_c. This important point is made clear by the middle data set presenting the temperatures associated with the onset of superconducting fluctuations which lie somewhere between T^* and T_c. This data set underlines the observation, consistent with the present calculations, that fluctuation transport effects are only apparent at temperatures well away from T^* but distinguished as well from T_c.

Comparison with equilibrated superconducting fluctuations

An important calibration of the conductivity theory here is to compare with earlier equilibrium data (here for the cuprates), which is presented in two different references[56,58] addressing the near-T_c fluctuation contribution to $\sigma(\omega)$ for microwave[56] and THz frequencies[58]. A key summary plot focuses on the angle $\phi = \tan^{-1}(\frac{\sigma_2}{\sigma_1})$ as a function of frequency, which can be more directly compared. This is particularly useful as the broad quasi-particle background was deliberately removed in experiment[56] so that this provides

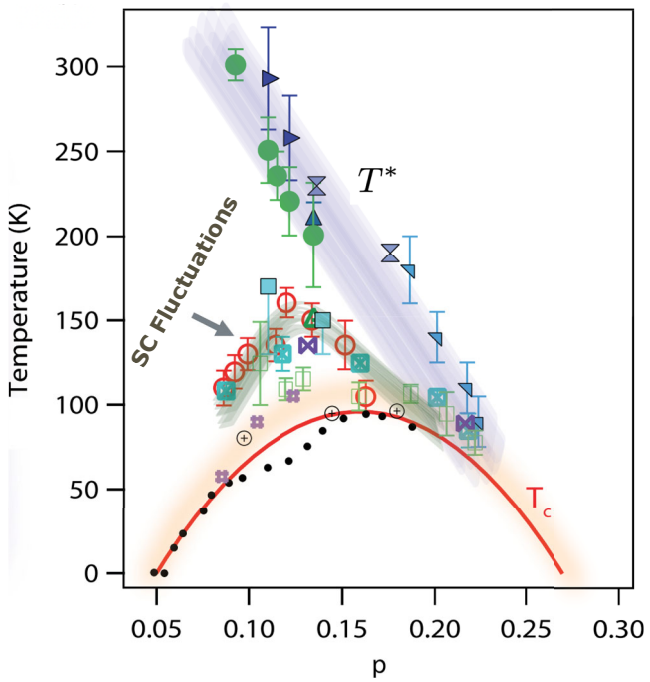

Fig. 6 | Summary of cuprate data and the various energy scales which are prototypical in BCS-BEC theory. The temperature T^* represents the opening of a fermionic gap and is not directly relevant to bosonic transport, as this requires a very small pair chemical potential. Enhanced fluctuation transport of interest in this paper, thus, takes place closer to T_c as indicated in the figure[60]. This temperature scale is consistent with the regime in Fig. 2b where the bosonic chemical potential μ_{pair} is sufficiently small: $\mu_{\text{pair}} \ll T_c$.

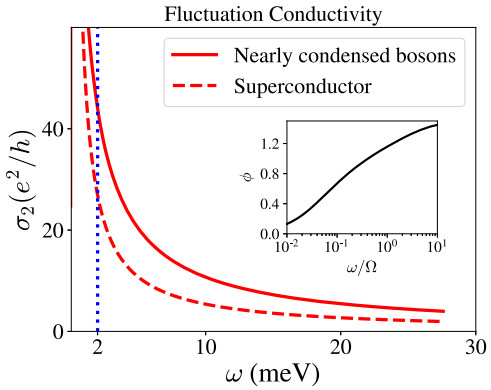

Fig. 7 | This figure shows the behavior of preformed pairs which contribute to σ_2, as *equilibrium* superconducting fluctuations and the contrast with a true ordered superconductor. Here $T = 1.2T_c$ and we presume $T^*/T_c = 15$. The inset plots the angle $\phi = \tan^{-1}(\frac{\sigma_2}{\sigma_1})$ and makes a connection to fluctuation experiments in Refs. 56 and 58. Here, Ω is arbitrary and chosen to be 1 meV. The blue vertical line shows the lower limit accessible experimentally.

access to the transport properties with negligible fermion contributions, much like in the Eliashberg scenario.

Plotted in Fig. 7 is the fluctuation contribution associated with the pairs, which can be more directly compared to another class of experiments[56,58]. Here we indicate the frequency-dependent behavior of σ_2 at $T = 1.2T_c$ as compared with an ideal superconductor (with superfluid fraction $\frac{n_s}{n} = 0.6$). Indeed, the plot shows that this normal state transport is rather similar to that of the actual superconductor for temperatures near T_c.

The inset plots the angle $\phi = \tan^{-1}(\frac{\sigma_2}{\sigma_1})$ and this behavior is seen to be semi-quantitatively similar to that found experimentally (see Fig. 3 in Ref. 56 and Fig. 3 in Ref. 58). Since we have argued that the fermion contributions to the ac conductivity are negligible in the light-induced preformed pair phase, these experimental figures serve to nicely characterize this rather new phase of quantum matter.

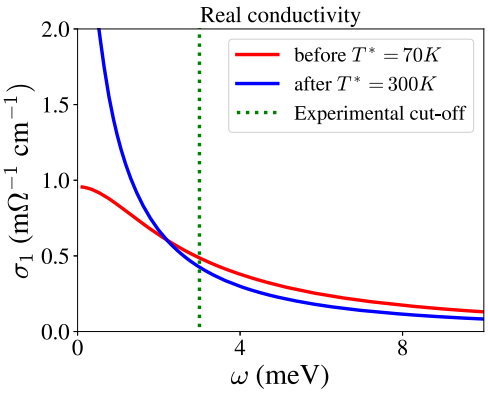

Fig. 8 | This figure plots the real part of the conductivity before and after exposure to light. Over the range of measured frequencies one can see that there is very little change, even less than observed for the imaginary contribution which is plotted in Fig. 3. One should note that these two figures are plotted over different ranges of frequency, however.

Finally, for completeness it is useful to present the plot in Fig. 8 showing the real contribution to the conductivity before and after exposure to light. Note that there is very little change and very little suppression of the real part of the conductivity over the range of measured frequencies. This can be compared with the behavior observed for the imaginary contribution which is plotted (over a different frequency scale) in Fig. 3, where the change is more significant.

Data availability

The data analyzed in the current study are available from the author Ke Wang on reasonable request.

Code availability

The codes used for the current study are available from the author Ke Wang on reasonable request.

Received: 13 December 2024; Accepted: 11 June 2025;
Published online: 03 July 2025

References

1. Mankowsky, R. et al. Nonlinear lattice dynamics as a basis for enhanced superconductivity in $YBa_2Cu_3O_{6.5}$. *Nature* **516**, 71–73 (2014).
2. Tang, R., Boi, F. & Cheng, Y.-H. Light-induced topological phase transition via nonlinear phononics in superconductor CsV_3Sb_5. *npj Quantum Mater* **8**, 78 (2023).
3. Orenstein, J. Ultrafast spectroscopy of quantum materials. *Phys. Today* **65**, 44–50 (2012).
4. Nicoletti, D. & Cavalleri, A. Nonlinear light–matter interaction at terahertz frequencies. *Adv. Opt. Photonics* **8**, 401–464 (2016).
5. Cavalleri, A. Photo-induced superconductivity. *Contemp. Phys.* **59**, 31–46 (2018).
6. Demsar, J. Non-equilibrium phenomena in superconductors probed by femtosecond time-domain spectroscopy. *J. Low. Temp. Phys.* **201**, 676–709 (2020).
7. De La Torre, A. et al. Colloquium: Nonthermal pathways to ultrafast control in quantum materials. *Rev. Mod. Phys.* **93**, 041002 (2021).
8. Uemura, Y. J. Dynamic superconductivity responses in photoexcited optical conductivity and Nernst effect. *Phys. Rev. Mater.* **3**, 104801 (2019).

9. Nava, A., Giannetti, C., Georges, A., Tosatti, E. & Fabrizio, M. Cooling quasiparticles in A_3C_{60} fullerides by excitonic mid-infrared absorption. *Nat. Phys.* **14**, 154–159 (2018).
10. Dolgirev, P. E. et al. Periodic dynamics in superconductors induced by an impulsive optical quench. *Commun. Phys.* **5**, 234 (2022).
11. Salvador, A. G. et al. Principles of 2D terahertz spectroscopy of collective excitations: the case of Josephson plasmons in layered superconductors. *Phys. Rev. B.* **110**, 094514 (2024).
12. Knap, M., Babadi, M., Refael, G., Martin, I. & Demler, E. Dynamical Cooper pairing in nonequilibrium electron-phonon systems. *Phys. Rev. B*. **94**, 214504 (2016).
13. Babadi, M., Knap, M., Martin, I., Refael, G. & Demler, E. Theory of parametrically amplified electron-phonon superconductivity. *Phys. Rev. B.* **96**, 014512 (2017).
14. Raines, Z. M., Stanev, V. & Galitski, V. M. Enhancement of superconductivity via periodic modulation in a three-dimensional model of cuprates. *Phys. Rev. B*. **91**, 184506 (2015).
15. Kim, M. et al. Enhancing superconductivity in A_3C_{60} fullerides. *Phys. Rev. B.* **94**, 155152 (2016).
16. Komnik, A. & Thorwart, M. BCS theory of driven superconductivity. *Eur. Phys. J. B.* **89**, 1–5 (2016).
17. Okamoto, J., Cavalleri, A. & Mathey, L. Theory of enhanced interlayer tunneling in optically driven high-T_c superconductors. *Phys. Rev. Lett.* **117**, 227001 (2016).
18. Sentef, M. Light-enhanced electron-phonon coupling from nonlinear electron-phonon coupling. *Phys. Rev. B.* **95**, 205111 (2017).
19. Coulthard, J., Clark, S. R., Al-Assam, S., Cavalleri, A. & Jaksch, D. Enhancement of superexchange pairing in the periodically driven Hubbard model. *Phys. Rev. B*. **96**, 085104 (2017).
20. Kennes, D. M., Wilner, E. Y., Reichman, D. R. & Millis, A. J. Transient superconductivity from electronic squeezing of optically pumped phonons. *Nat. Phys.* **13**, 479–483 (2017).
21. Mazza, G. & Georges, A. Nonequilibrium superconductivity in driven alkali-doped fullerides. *Phys. Rev. B*. **96**, 064515 (2017).
22. Murakami, Y., Tsuji, N., Eckstein, M. & Werner, P. Nonequilibrium steady states and transient dynamics of conventional superconductors under phonon driving. *Phys. Rev. B*. **96**, 045125 (2017).
23. Sentef, M. et al. Theory of Floquet band formation and local pseudospin textures in pump-probe photoemission of graphene. *Nat. Commun.* **6**, 7047 (2015).
24. Dasari, N. & Eckstein, M. Transient Floquet engineering of superconductivity. *Phys. Rev. B.* **98**, 235149 (2018).
25. Wang, Y., Chen, C.-C., Moritz, B. & Devereaux, T. Light-enhanced spin fluctuations and d-wave superconductivity at a phase boundary. *Phys. Rev. Lett.* **120**, 246402 (2018).
26. Tindall, J. et al. Dynamical order and superconductivity in a frustrated many-body system. *Phys. Rev. Lett.* **125**, 137001 (2020).
27. Jotzu, G. et al. Superconducting fluctuations observed far above T_c in the isotropic superconductor K_3C_{60}. *Phys. Rev. X* **13**, 021008 (2023).
28. Chen, Q., Wang, Z., Boyack, R., Yang, S. & Levin, K. When superconductivity crosses over: From BCS to BEC. *Rev. Mod. Phys.* **96**, 025002 (2024).
29. Chen, Q., Stajic, J., Tan, S. & Levin, K. BCS–BEC crossover: From high temperature superconductors to ultracold superfluids. *Phys. Rep.* **412**, 1–88 (2005).
30. Eliashberg, G. M. Film superconductivity stimulated by a high-frequency field. *Tech. Rep. Inst. of Theoretical Physics, Moscow* **11**, 114–116 (1970).
31. Klapwijk, T. & de Visser, P. The discovery, disappearance and re-emergence of radiation-stimulated superconductivity. *Ann. Phys.* **417**, 168104 (2020).
32. Robertson, A. & Galitski, V. M. Nonequilibrium enhancement of cooper pairing in cold fermion systems. *Phys. Rev. A* **80**, 063609 (2009).
33. Heslinga, D. & Klapwijk, T. Enhancement of superconductivity far above the critical temperature in double-barrier tunnel junctions. *Phys. Rev. B*. **47**, 5157 (1993).
34. Tredwell, T. & Jacobsen, E. Phonon-induced enhancement of the superconducting energy gap. *Phys. Rev. Lett.* **35**, 244 (1975).
35. Tredwell, T. & Jacobsen, E. Phonon-induced increase in the energy gap of superconducting films. *Phys. Rev. B*. **13**, 2931 (1976).
36. Johnston, S. et al. Systematic study of electron-phonon coupling to oxygen modes across the cuprates. *Phys. Rev. B* **82**, 064513 (2010).
37. Isoyama, K. et al. Light-induced enhancement of superconductivity in iron-based superconductor $FeSe_{0.5}Te_{0.5}$. *Commun. Phys.* **4**, 160 (2021).
38. Buzzi, M. et al. Phase diagram for light-induced superconductivity in κ-$(ET)_2$-X. *Phys. Rev. Lett.* **127**, 197002 (2021).
39. Mitrano, M. et al. Possible light-induced superconductivity in K_3C_{60} at high temperature. *Nature* **530**, 461–464 (2016).
40. Ren, M. et al. Direct observation of full-gap superconductivity and pseudogap in two-dimensional fullerides. *Phys. Rev. Lett.* **124**, 187001 (2020).
41. Nakagawa, Y. et al. Gate-controlled BCS-BEC crossover in a two-dimensional superconductor. *Science* **372**, 190–195 (2021).
42. Park, J. M., Cao, Y., Watanabe, K., Taniguchi, T. & Jarillo-Herrero, P. Tunable strongly coupled superconductivity in magic-angle twisted trilayer graphene. *Nature* **590**, 249–255 (2021).
43. Kadanoff, L. P. & Martin, P. C. Theory of many-particle systems. II. Superconductivity. *Phys. Rev.* **124**, 670–697 (1961).
44. Tikhonov, K. S., Semenov, A. V., Devyatov, I. A. & Skvortsov, M. A. Microwave response of a superconductor beyond the Eliashberg theory. *Ann. Phys.* **417**, 168101 (2020).
45. Nozières, P. & Schmitt-Rink, S. Bose condensation in an attractive fermion gas: From weak to strong coupling superconductivity. *J. Low. Temp. Phys.* **59**, 195–211 (1985).
46. Tan, S. & Levin, K. Nernst effect and anomalous transport in cuprates: A preformed-pair alternative to the vortex scenario. *Phys. Rev. B.* **69**, 064510 (2004).
47. Larkin, A. & Varlamov, A.*Theory of fluctuations in superconductors*, vol. 127 (OUP Oxford, 2005).
48. Suzuki, Y. et al. Mott-driven BEC-BCS crossover in a doped spin liquid candidate κ-(BEDT- TTF)$_4$ $Hg_{2.89}$ Br_8. *Phys. Rev. X* **12**, 011016 (2022).
49. Dodge, J. S., Lopez, L. & Sahota, D. G. Optical saturation produces spurious evidence for photoinduced superconductivity in K_3 C_{60}. *Phys. Rev. Lett.* **130**, 146002 (2023).
50. Dodge, J. S., Lopez, L. & Sahota, D. G. Status of the spurious evidence for photoinduced superconductivity. In *2023 48th International Conference on Infrared, Millimeter, and Terahertz Waves (IRMMW-THz)*, 1–2 (IEEE, 2023).
51. Liu, B. et al. Pump frequency resonances for light-induced incipient superconductivity in $YBa_2Cu_3O_{6.5}$. *Phys. Rev. X* **10**, 011053 (2020).
52. Fava, S. et al. Magnetic field expulsion in optically driven $YBa_2Cu_3O_{6.48}$. *Nature* **632**, 75–80 (2024).
53. Emery, V. J. & Kivelson, S. A. Importance of phase fluctuations in superconductors with small superfluid density. *Nature* **374**, 434–7 (1995).
54. Li, L. et al. Diamagnetism and cooper pairing above T_c in cuprates. *Phys. Rev. B* **81**, 054510 (2010).
55. Kubo, R. & Obata, Y. Note on the paramagnetic susceptibility and the gyromagnetic ratio in metals. *J. Phys. Soc. Jpn.* **11**, 547–550 (1956).
56. Corson, J., Mallozzi, R., Orenstein, J., Eckstein, J. N. & Bozovic, I. Vanishing of phase coherence in underdoped $Bi_2Sr_2CaCu_2O_{8+\delta}$. *Nature* **398**, 221–223 (1999).
57. Boyack, R., Chen, Q., Varlamov, A. & Levin, K. Cuprate diamagnetism in the presence of a pseudogap: Beyond the standard fluctuation formalism. *Phys. Rev. B*. **97**, 064503 (2018).

58. Bilbro, L. et al. Temporal correlations of superconductivity above the transition temperature in La_{2-x} Sr_x CuO_4 probed by terahertz spectroscopy. *Nat. Phys.* **7**, 298–302 (2011).
59. Hashimoto, M., Vishik, I. M., He, R.-H., Devereaux, T. P. & Shen, Z.-X. Energy gaps in high-transition-temperature cuprate superconductors. *Nat. Phys.* **10**, 483–495 (2014).
60. Vishik, I. Photoemission perspective on pseudogap, superconducting fluctuations, and charge order in cuprates: a review of recent progress. *Rep. Prog. Phys.* **81**, 062501 (2018).

Acknowledgements

We thank Steve Dodge, Andrea Cavalleri, and Andrew Higginbotham for very helpful discussions and communications. Z. W. and Q. C. are supported by the Innovation Program for Quantum Science and Technology (Grant No. 2021ZD0301904). We also acknowledge the University of Chicago's Research Computing Center for their support of this work.

Author contributions

K.L. conceived and supervised the project. K.W. performed the computations. K.W., Q.C. and Z.W. contributed to the acquisition of the data and preparation of figures. All authors have contributed to the interpretation of the data and the drafting as well as the revision of the manuscript.

Competing interests

The authors declare no competing interests.

Additional information

Correspondence and requests for materials should be addressed to Ke Wang.